Chemometrics and Intelligent Laboratory Systems 148 (2015) 60–71

Contents lists available at ScienceDirect

Chemometrics and Intelligent Laboratory Systems

journal homepage: www.elsevier.com/locate/chemolab

Multidimensional voltammetry: Four-way multivariate calibration with third-order differential pulse voltammetric data for multi-analyte quantification in the presence of uncalibrated interferences

Ali R. Jalalvand [a,b,*], Mohammad-Bagher Gholivand [a,*], Hector C. Goicoechea [b]

[a] Department of Analytical Chemistry, Faculty of Chemistry, Razi University, Kermanshah 671496734, Iran
[b] Laboratorio de Desarrollo Analítico y Quimiometría (LADAQ), Cátedra de Química Analítica I, Universidad Nacional del Litoral, Ciudad Universitaria, CC 242 (S3000ZAA), Santa Fe, Argentina

ARTICLE INFO

Article history:
Received 18 April 2015
Received in revised form 29 July 2015
Accepted 2 September 2015
Available online 8 September 2015

Editor: P.K. Hopke

Keywords:
Four-way voltammetric array
Third-order multivariate calibration
U-PLS/RTL
N-PLS/RTL
Multi-analyte quantification
Uncalibrated interference

ABSTRACT

A four-way multivariate calibration approach based on the combination of differential pulse voltammetric (DPV) data and four-way algorithms is described for the first time. To achieve this goal, the DPV response of each sample was recorded thirty-six times. Six current-potential matrices were recorded at six different pulse durations. Each matrix consists of six vectors which have been recorded at six different pulse heights. The three-way data array obtained for the calibration set and for each of the test samples were joined into a single four-way data array. The recorded four-way data array was nonlinear, thus, the non-linearities were tackled by potential shift correction using correlation-optimized warping (COW) algorithm and subsequently was analyzed with unfolded-partial least squares/residual trilinearization (U-PLS/RTL) and multi-way-PLS/RTL (N-PLS/RTL) as third-order multivariate calibration algorithms. A comprehensive and systematic strategy for comparing the performance of the two algorithms was presented in this work, in particular with a view of practical applications. This comparison was developed to identify which algorithm offers the best predictions for the simultaneous determination of levodopa (LD), carbidopa (CD), methyldopa (MD), acetaminophen (AC), tramadol (TRA), lidocaine (LC), tolperisone (TOP), ofloxacin (OF), levofloxacin (LOF), and norfloxacin (NOF) in the presence of benserazide (BA), dopamine (DP), and ciprofloxacin (COF) as uncalibrated interferences using a multi-walled carbon nanotubes modified glassy carbon electrode (MWCNTs/GCE). This study demonstrated the more superiority of U-PLS/RTL to resolve the complex systems. The results of applying U-PLS/RTL for the simultaneous determination of the studied analytes in human serum samples as experimental cases were also encouraging.

1. Introduction

Calibration is the mathematical and statistical process of extracting information, usually analyte concentration, from an instrument signal [1]. Traditionally, the measurements have consisted of a single number (zero-order data). The concentrations of unknown samples can be predicted by regressing their measured signals against the standard calibration curve. However, a significant disadvantage of zero-order calibration is that a signal must be fully selective for the analyte of interest, which has led to the development of first-order multivariate calibration methods [2–13]. The data of measurements are a vector (first-order data), rather than just a single measurement as in the univariate case, thus, the first-order calibration has a number of advantages. These types of methods include partial least-squares (PLS) [2,3] and principal component regression (PCR) [8,12], which have become popular in recent years. It makes sense that when more data are available per sample, more information may be extracted. Therefore, it follows that if the data of measurements is a matrix (second-order data), even more advantages could be obtained by using second-order calibration (three-way calibration) methods. The primary advantage of these methods has been known as "second-order advantage" [14,15], it allows the analytes of interest to be quantitated even in the presence of uncalibrated interferences.

The higher-order calibration methods are not limited to the second-order calibration or the analysis of three-way data. Third-order calibration methods can also be used for the similar purpose and four-way data can be processed and interpreted in the similar way. In principle, the advantage of third-order calibration not only contains a similar second-order advantage that the components of interest can be determined even in the presence of uncalibrated interferences in complex samples, but also holds some additional advantages. The inclusion of an extra mode in the data increases the selectivity and sensitivity of the analysis by the inclusion of additional information of the sample. It can provide more information about the analytes than second-order calibration for an additional dimension introduced. The intrinsic profiles in each mode can be determined uniquely for every species in the prediction

* Corresponding authors. Tel.: +98 831 4274557; fax: +98 831 4274559.
E-mail addresses: ali.jalalvand1984@gmail.com (A.R. Jalalvand), mbgholivand2013@gmail.com (M.-B. Gholivand).

http://dx.doi.org/10.1016/j.chemolab.2015.09.003
0169-7439/

samples [16]. Because four-way data array cannot be obtained conveniently, only several works have been reported for third-order calibration [17–23].

Levodopa (LD) is a precursor of the neurotransmitter dopamine, widely used in the clinical treatment of Parkinson's disease [24]. It could be converted to dopamine (DP) by dopamine decarboxylase and capable of crossing the protective blood-brain barrier, whereas DP itself cannot. To avoid adverse reactions caused by elevated levels of dopamine in peripheral tissues, LD is often administered in combination with carbidopa (CD), an inhibitor of the decarboxylase enzyme, which does not cross the blood-brain barrier. Methyldopa (MD), which is an old antihypertensive agent, is converted to 1-methyl dopamine and 1-methyl norepinephrine [25]. In addition, the United State Pharmacopoeia (USP) specifies MD as one of the most important impurities in the analysis of levodopa–carbidopa (LD-CD) combination formulation [26]. Changes in the concentration of these drugs in the body may influence the bioavailability and biopharmaceutical properties of the pharmaceutical preparation and, subsequently, their magnitude of action. Thus, the determination of LD and its inhibitors and impurities in biological fluids has an essential role in the diagnostics of diseases related to them. Acetaminophen (AC) is a long-established substance being one of the most extensively employed drugs in the world. It is also found that overdoses of AC will damage liver and kidney. It has been found that human absorption of AC is very dependent on gastric emptying. Other drugs that alter gastric emptying can change the pharmacokinetics of AC. It has been shown that LD can influence gastric emptying [27]. Therefore it would be useful to study simultaneous determination of AC and LD [27]. Tramadol (TRA) is a centrally acting opioid analgesic, used in treating moderate to severe pain. In combination with opioid analgesics (viz., TRA), AC can also be used in the management of severe post-surgical pain and providing palliative care in advanced cancer patients [28]. However, their overdose is toxic in nature and may cause dizziness, nausea, and vomiting [28]. Therefore, the development of a sensitive and selective method for simultaneous determination of TRA and AC is highly desirable for analytical applications and diagnostic research. Therefore, interest in the development of a simple method for the simultaneous determination of LD, CD, MD, TRA, and AC continues.

Lidocaine (LC) is widely used as a local anesthetic. It has also achieved prominence as an antiarrhythmic agent and is now in common use particularly as emergency treatment for ventricular arrhythmias that are encountered after cardiac surgery or acute myocardial infection. A notable side effect of LC maybe caused by its metabolites rather than LC itself [29]. To the best of our knowledge, there is only one report on the simultaneous determination of TRA and LC [29]. Tolperisone (TOP) is a centrally acting muscle relaxant that is used for relieving spasticity of neurological origin and muscle spasms associated with painful locomotor diseases [30–32]. Only a few reports have been described in the literatures on the analytical methods for the simultaneous determination of TOP and LC [33]. Therefore, the development of a sensitive and selective method for the simultaneous determination of LD, CD, MD, TRA, AC, LC, and TOP is highly desirable for analytical applications and diagnostic research.

Many new fluoroquinolone derivatives have been developed because of their potent and wide-spectrum antimicrobial activities, and good clinical efficacy [34]. Among the fluoroquinolones, in particular, ofloxacin (OF), norfloxacin (NOF), and levofloxacin (LOF) are frequently used for the treatment of various types of microbial infections. Therefore, from a clinical point of view, simultaneous determination of these fluoroquinolones is important. To the best of our knowledge, there is only one report on the simultaneous determination of TRA, LC, and OF, and they have claimed fast analysis of TRA, LC, and OF is of clinic importance for understanding the patient's medical process. Therefore, the development of a sensitive and selective method for the simultaneous determination of LD, CD, MD, TRA, AC, LC, TOP, OF, NOF, and LOF is highly desirable for analytical applications and diagnostic research.

The oxidation peak potential for benserazide (BA) is very close to LD, CD, and MD, oxidation peak potential for dopamine (DP) is very close to AC, and oxidation peak potential for ciprofloxacin (COF) is very close to OF, NOF, and LOF. Consequently, BA, DP, and COF are regarded as uncalibrated interferences in the simultaneous determination of LD, CD, MD, TRA, AC, LC, TOP, OF, NOF, and LOF.

In the present work, we reported a simple method based on changes in the pulse height and pulse duration of DPV signals to create a four-way voltammetric data array. Also, we show the capability of U-PLS and N-PLS to handle voltammetric data, in combination with RTL, to determine ten analytes in the presence of three unexpected interferences. Finally, U-PLS/RTL was chosen for the analysis of the electrochemical responses of the MWCNTs/GCE sensor for the simultaneous determination of ten analytes in human serum samples (Scheme 1). To the best of our knowledge, this work is the first report on exploiting second-order advantage from third-order DPV data for the simultaneous determination of ten analytes in the presence of three unexpected interferences.

2. Experimental and theoretical details

2.1. Chemicals, solutions, softwares, and instrumentation

LD (Sigma), CD (SERVA), MD (Sigma–Aldrich), AC (Sigma–Aldrich), TRA (Fluka), LC (Sigma), TOP (SERVA), OF (Sigma), LOF (Fluka), NOF (Sigma), BA (USPlabs), DP (Sigma), COF (Fluka), and MWCNTs (Sigma–Aldrich) were used as received. All other reagents and materials were of analytical grade from legal sources. All the solutions were prepared using double-distilled water (DDW). A phosphate buffer solution (PBS, 0.1 mol L^{-1}) of pH 3.0 was prepared using Na_2HPO_4 and NaH_2PO_4 and served as a supporting electrolyte solution (pH adjustment was carried out by NaOH and H_3PO_4). The MWCNTs were purified according to the method reported previously [35]. In brief, 50 mg of carbon nanotubes were dispersed in 60 mL of 2.2 M HNO_3 and ultrasonicated for 30 min and the suspension was then kept at room temperature for 20 h. The MWCNTs were then filtered, washed with DDW to neutrality, and dried at 37 °C in an oven. All the recorded electrochemical data were smoothed, when necessary, and converted to data matrices by the use of several home-made m-files in MATLAB environment (Version 7.14, MathWorks, Inc.). All the routines used in this study were run in the MATLAB environment. Electrochemical experiments were performed using a μ-Autolab TYPE III, Eco Chemie BV, Netherlands, equipped with PSTA 20 model and driven by NOVA 1.8 software. A three-electrode system was used in the experiment including a modified glassy carbon electrode as working electrode, an Ag/AgCl electrode (saturated KCl) as reference electrode, and a Pt wire as counter-electrode. The electrochemical impedance spectroscopic (EIS) experiments were carried out using the same three-electrode configuration above on the mentioned Autolab in a supporting electrolyte solution of 1.0 M KCl containing equimolar $[Fe(CN)_6]^{4-/3-}$ in a frequency range from 0.1 to 100.0 kHz. The fit and simulation of equivalent circuit were analyzed with FRA software. The scanning electron microscopic (SEM) experiments were performed by a KYKY-EM 3200 scanning electron microscope. A JENWAY-3345 pH-meter equipped with a combined glass electrode was used to pH measurements. All measurements were performed at room temperature. All computations were performed on a DELL XPS laptop (L502X) with Intel Core i7-2630QM 2.0GHz, 8 GB of RAM and Windows 7-64 as its operating system.

2.2. Preparation of the MWCNTs/GCE

The bare GCE was polished carefully using zinc oxide and alumina mixture with the help of a silky pad. The polished electrode was washed with DDW and then dried. A suspension of the purified MWCNTs (0.5 mg/ml) in DMF was prepared by the dispersion of

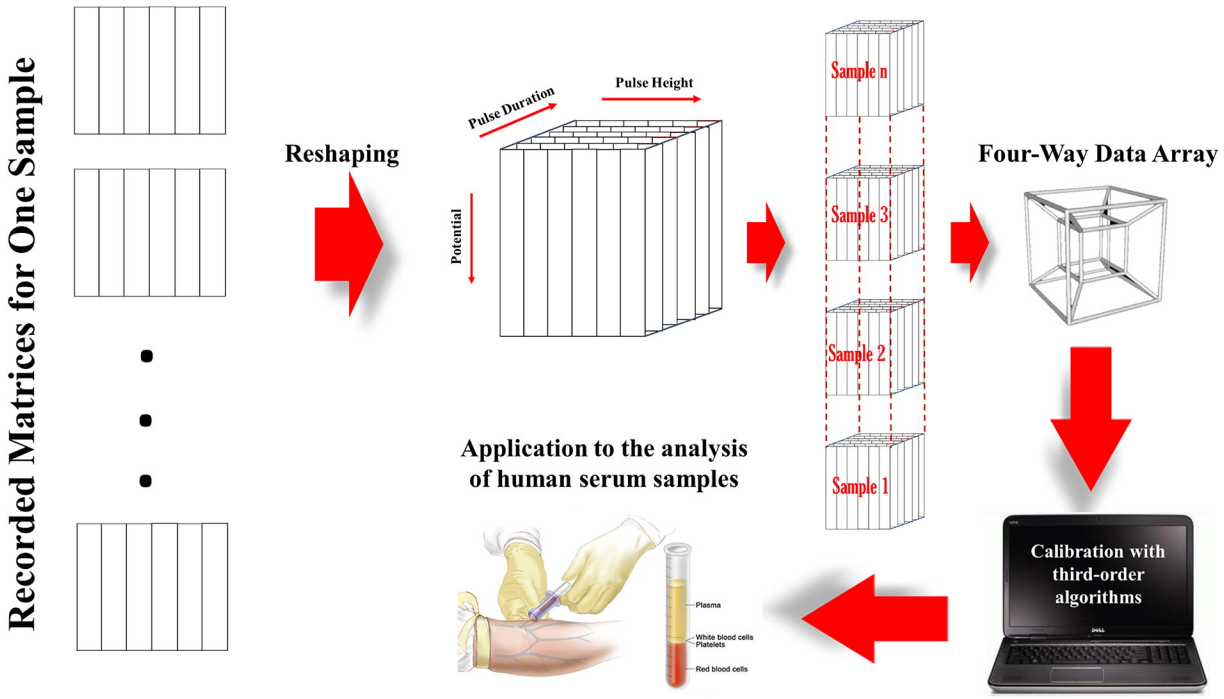

Scheme 1. Schematic representation of the developed methodology in this work.

MWCNTs using ultrasonic churning. Small amount (40 μl) of this suspension was put on the surface of bare polished GCE. It was seen that the suspension covered total surface area of the GCE. The suspension was allowed to desiccate by keeping the electrode in open at room temperature. Within about half an hour, the solvent evaporated off leaving a thin layer of MWCNTs all around the electrode surface. This process was repeated a number of times till a smooth layer formed all around the electrode surface. The electrode so obtained is called MWCNTs/GCE.

2.3. Preparation of real samples

A human serum sample which was provided by a medical diagnostic laboratory in Kermanshah, Iran, was used as an experimental case to evaluate the performance of the proposed methodology. According to the method of Shu et al. [36], to eliminate protein and other substances, 5.0 mL of human serum sample was placed in a 10.0 mL glass tube and 1.0 mL of 15.0% (w/v) zinc sulfate solution-acetonitrile (50/40, v/v) was added. The glass tube was vortexed for 20.0 min, maintained at 4.0 °C for 15.0 min followed by centrifugation at 4000.0 rpm for 5.0 min. Then, the supernatant was collected in the same tube and this solution was used for subsequent analyses.

2.4. Generating third-order DPV data

In this work, the pulse heights (ΔE) and pulse durations (τ) in DPV signals were changed to obtain third-order DPV data. The theory behind the proposed procedure will be briefly discussed. The current signal intensity in DPV can be obtained using the following equations [37]:

$$\delta_i = \frac{nFAD_O^{1/2}C_O^*}{\pi^{1/2}(\tau\text{-}\tau')^{1/2}}\left[\frac{P_A(1\text{-}\sigma^2)}{(\sigma+P_A)(1+P_A\sigma)}\right] \quad (1)$$

$$P_A = \xi \exp\left[\frac{nF}{RT}\left(E+\frac{\Delta E}{2}\text{-}E^{0'}\right)\right] \quad (2)$$

$$\sigma = \exp\left(\frac{nF}{RT}\frac{\Delta E}{2}\right) \quad (3)$$

$$\xi = \left(\frac{D_O}{D_R}\right)^{1/2} \quad (4)$$

where, ΔE and τ are pulse height and pulse duration, respectively, and other symbols have their conventional meanings. For a typical electrochemical reaction, third-order voltammetric data can be obtained by sweeping potentials at different pulse heights and pulse durations. For each sample, six pulse durations of 0.0078–0.0468 s with a 0.0078 s interval were assigned, and for each pulse duration, six voltammograms were recorded at six different pulse heights of 0.0031–0.0191 V with a 0.0031 V interval and on the whole for each sample six matrices (each matrix contains six vectors) have been recorded. These six matrices were then mathematically assembled using MATLAB commands to obtain a three-way array for each sample. The three-way data obtained for the calibration set and for each of the test samples were joined into a single four-way data array.

Literature survey revealed that change of ΔE can cause non-linearity in the recorded DPV data while change of τ doesn't cause any non-linearity [38,39]. Therefore, it is reasonable to have a non-bilinear (change in ΔE) and trilinear (change in τ) three-way data array for each sample and finally a non-quadrilinear (change in concentration for sample to sample) four-way data array.

2.5. Correlation optimized warping (COW)

The COW algorithm is also based on a piece-wise linear correction function, but unlike icoshift, it is continuous and made up of segments whose slope is allowed to take a limited number of discrete values determined by the length ℓ of the interval in which the voltammograms are divided and the maximum number of scan points, s, by which the length of each interval is allowed to change [40]. When the slope of a segment of the correction function $f(t_y)$ is not one, the corresponding intervals in sample and target contain a different number of points, and linear interpolation is used so that the interval in the sample is compressed or expanded to the same length as the corresponding interval in the target. The optimized cost function is the sum of the Pearson's correlation coefficient for all segments after interpolation and dynamic

programming is used to attain the global maximum given the constraints. Typically, a maximum allowed correction is set to further reduce the feasible region for $f(t_y)$. One known problem of the standard COW method is that, close to the endpoints, the maximum correction allowed by the slope constraints is reduced. While it is possible to modify the algorithm to account for this, a computationally more intensive but equally effective solution is to attach zeroes at both ends of the signals so that the necessary flexibility is guaranteed (namely, $\mathbf{w}_{max}/s^{-1}$ zeroes should be attached at each end). It is worth mentioning, that, while COW also allows for custom intervals, here its commonest format is used in which sample and target are divided in segments of equal length.

2.6. U-PLS/RTL

For four-way calibration, U-PLS/RTL constitutes an extension of U-PLS/RBL one further mode [19] and will be briefly described in this section. When using four-way data, in the U-PLS method, the original matrix data are transformed into one-dimensional arrays (vectors) by concatenating (unfolding) the original three-dimensional information, and concentration information is first employed into the calibration step (without including data for the unknown sample) [41]. The calibration third-order arrays are vectorized (unfolded) and a usual U-PLS model is calibrated with these data and the vector of calibration concentrations $\mathbf{y}$ ($I \times 10$). This provides a set of loadings $\mathbf{P}$ and weight loadings $\mathbf{W}$ (both of size $JKL \times A$, where A is the number of latent factors), as well as regression coefficients $\mathbf{v}$ (size $A \times 10$). The parameter A can be selected by techniques such as leave-one-outcross-validation [42]. If no unsuspected interferences occur in the test sample, $\mathbf{v}$ can be employed to estimate the analyte concentration:

$$\mathbf{y}_u = \mathbf{t}_u^T \mathbf{v} \tag{5}$$

where $\mathbf{t}_u$ (size $A \times 1$) is the test sample score, obtained by a projection of the (unfolded) data for the test sample $\underline{\mathbf{X}}_u[\mathrm{vec}(\underline{\mathbf{X}}_u), \mathrm{size}(JKL \times 1)]$ onto the space of the A latent factors:

$$\mathbf{t}_u = \left(\mathbf{W}^T\mathbf{P}\right)^{-1}\mathbf{W}^T\mathbf{vec}(\underline{\mathbf{X}}_u) \tag{6}$$

When uncalibrated constituents occur in $\underline{\mathbf{X}}_u$, the sample scores given by Eq. (6) are not suitable for analyte prediction using Eq. (5). In this case, the residuals of the U-PLS prediction step will be abnormally large in comparison with the typical instrumental noise assessed by replicate measurements:

$$\begin{aligned}\mathbf{S}_p &= \|\mathrm{vec}(\mathbf{E}_p)\|/(JKL-A)^{1/2} \\ &= \left\|\mathrm{vec}(\underline{\mathbf{X}}_u) - \mathbf{P}\left(\mathbf{W}^T\mathbf{P}\right)^{-1}\mathbf{W}^T\mathrm{vec}(\underline{\mathbf{X}}_u)\right\|/(JKL-A)^{1/2} \\ &= \|\mathrm{vec}(\underline{\mathbf{X}}_u) - \mathbf{P}\mathbf{t}_u\|/(JKL-A)^{1/2}\end{aligned} \tag{7}$$

where $\|\cdot\|$ indicates the Euclidean norm, and JKL-A corresponds to the degree of freedom (number of variables minus number of adjustable parameters).

If interferent components occur in the test sample, the situation can be handled by RTL, based on a Tucker3 decomposition that models the interferent effects, as already described [19]. RTL aims at minimizing the norm of the residual vector $\mathbf{e}_u$, computed while fitting the sample data to the sum of the relevant contributions to the sample signal. For a single interferent, the relevant expression is

$$\mathrm{vec}(\underline{\mathbf{X}}_u) = \mathbf{P}\mathbf{t}_u + \mathbf{g}_{int}(\mathbf{d}_{int} \otimes \mathbf{c}_{int} \otimes \mathbf{b}_{int}) + \mathbf{e}_u \tag{8}$$

where $\mathbf{b}_{int}$, $\mathbf{c}_{int}$, and $\mathbf{d}_{int}$ are normalized profiles in the three modes for the interference and $\mathbf{g}_{int}$ is the first core element obtained for Tucker3 analysis of $\underline{\mathbf{E}}_p$ in the following way:

$$(\mathbf{g}_{int}, \mathbf{b}_{int}, \mathbf{c}_{int}, \mathbf{d}_{int}) = \mathrm{Tucker3}(\underline{\mathbf{E}}_p) \tag{9}$$

During this RTL procedure, $\mathbf{P}$ is kept constant at the calibration values and $\mathbf{t}_u$ is varied until $\|\mathbf{e}_u\|$ is minimized. The minimization can been carried out using either a Gauss–Newton (GN) procedure or an alternating least squares algorithm, in both cases starting with $\mathbf{t}_u$ from Eq. (6). Once $\|\mathbf{e}_u\|$ is minimized in Eq. (8), the analyte concentrations are provided by Eq. (5), by introducing the final $\mathbf{t}_u$ vector found by the RTL procedure.

The number of interferences N_i can be assessed by comparing the final residuals $\mathbf{s}_u$ with the instrumental noise level:

$$\mathbf{s}_u = \|\mathbf{e}_u\|/[JKL-(N_c+N_i)]^{1/2} \tag{10}$$

where $\mathbf{e}_u$ is from Eq. (8) and N_c is the number of calibrated analytes. Typically, a plot of $\mathbf{s}_u$ computed for trial number of components will show decreasing values, starting at $\mathbf{s}_p$ when the number of components is equal to A (the number of latent variables used to described the calibration data), until it stabilizes at a value compatible with the experimental noise, allowing to locate the correct number of components.

To analyze the presently discussed data, the Tucker3 model in Eq. (9) is constructed by restricting the loadings to be orthogonal, and with no special constraints on the core elements. For a single unexpected component, this analysis is straightforward and provides the corresponding interferent profiles in the three modes. For additional unexpected constituents, several different Tucker3 models could in principle be constructed, because the number of loadings may be different in each mode. We notice that the aim which guides the RTL procedure is the minimization of the residual error term $\mathbf{s}_u$ of Eq. (10) to a level compatible with the degree of noise present in the measured signals. Therefore, if two unexpected components are considered, for example, one should explore the possible Tucker3 models having one or two loadings in each mode, and select the simplest model giving a residual value of $\mathbf{s}_u$ which is not statistically different than the minimum one. For more unexpected components, a similar procedure is recommended. The final Tucker3 model selected to model the unexpected effects is the simplest one which provides a value of $\mathbf{s}_u$ which is not statistically different than the noise level.

We note that two different residual parameters appear in the above discussion, which should not be confused: $\mathbf{s}_p$ [Eq. (7)] corresponds to the difference between the test sample signal and that model by U-PLS before the RTL procedure, while $\mathbf{s}_u$ [Eq. (10)] arises from the difference after the RTL modeling of the interferent effects. Hence, it is the latter one which should be comparable to the instrumental noise level if RTL is successful.

2.7. N-PLS/RTL

In the N-PLS method applied to third-order data, concentration information is employed in the calibration step, without including data for the unknown sample. The I calibration data arrays, together with the vector of calibration concentrations $\mathbf{y}$ ($I \times 1$), are employed to obtain sets of loadings $\mathbf{W}^j$, $\mathbf{W}^k$, and $\mathbf{W}^l$ (of sizes $J \times A$, $K \times A$, and $L \times A$, where A is the number of latent factors), as well as regression coefficients $\mathbf{b}$ (size $A \times 1$) [43]. The parameter A can be selected by techniques such as leave-one-outcross-validation [42]. If no unexpected components occurred in the test sample, $\mathbf{b}$ could be employed to estimate the analyte concentration according to:

$$\mathbf{y}_u = \mathbf{t}_u^T \mathbf{b} \tag{11}$$

where $\mathbf{t}_u$ is the test sample score vector, obtained by appropriate projection of the test data onto the calibration loading matrices ($\mathbf{t}_u = (\mathbf{P}^T\mathbf{W})^{-1}\mathbf{P}^T\mathbf{X}_u$). When unexpected constituents occur in the unknown sample, the latter scores are unsuitable for analyte prediction through Eq. (11). In this case, it is useful to consider the residuals of the N-PLS modeling of the test sample signal [$\mathbf{s}_p$, see Eq. (12) below] before prediction is made. These residuals will be abnormally large in comparison with the typical instrumental noise level:

$$\mathbf{s}_p = \|\mathbf{e}_p\|/(JKL-A)^{1/2} = \left\|vec(\mathbf{X}_u) - vec\left(\hat{\mathbf{X}}_u\right)\right\|/(JKL-A)^{1/2} \quad (12)$$

where $\hat{\mathbf{X}}_u$ is the sample three-way data array ($\mathbf{X}_u$) reconstructed by the N-PLS model and $\|\cdot\|$ indicates the Euclidean norm.

This situation can be handled by a separate procedure called residual trilinearization, based on the Tucker3 model of the unexpected effects, as discussed above for U-PLS/RTL. In the case of N-PLS/RTL, the analogous expression to Eq. (8) is

$$\mathbf{X}_u = \text{reshape}\left\{\mathbf{t}_u\left[\left(\mathbf{W}^j|\otimes|\mathbf{W}^k\right)|\otimes|\mathbf{W}^l\right]\right\} + \text{Tucker3}\left(\hat{\mathbf{X}}_u - \mathbf{X}_u\right) + \mathbf{E}_u \quad (13)$$

where 'reshape' indicates transforming a $JKL \times 1$ vector into a $J \times K \times L$ three-way array, and $|\otimes|$ indicates the Kathri–Rao operator. During this RTL procedure, the weight loadings $\mathbf{W}_j$, $\mathbf{W}_k$, and $\mathbf{W}_l$ are kept constant at the calibration values, and $\mathbf{t}_u$ is varied until the final RTL residual error $\mathbf{s}_u$ is minimized using a Gauss–Newton procedure, with $\mathbf{s}_u$ given by:

$$\mathbf{s}_u = \|\mathbf{E}_u\|/[(JKL-(N_c+N_i)]^{1/2} \quad (14)$$

where $\mathbf{E}_u$ is from Eq. (13). Once this is done, the analyte concentrations are provided by Eq. (11), by introducing the final $\mathbf{t}_u$ vector found by the RTL procedure. The considerations discussed above concerning the Tucker3 model of Eq. (13) do also apply to N-PLS/RTL.

2.8. Model efficiency estimation

In order to evaluate the performance of U-PLS/RTL and N-PLS/RTL, each model was validated for the prediction of the test sets, evaluating root mean square errors of prediction (RMSEP), and relative error of prediction (REP).

$$\text{RMSEP} = \sqrt{\frac{\sum_1^n \left(y_{pred} - y_{act}\right)^2}{n}} \quad (15)$$

$$\text{REP}(\%) = \frac{100}{y_{mean}}\sqrt{\frac{1}{n}\sum_{i=1}^{n}\left(y_{pred} - y_{act}\right)^2} \quad (16)$$

where y_{act} and y_{pred} are actual and predicted concentrations of each component, respectively, and y_{mean} refers to the mean of the actual concentrations and n is the number of samples in test set.

2.9. Analytical figures of merit (AFOM)

A figure of merit is a quantity used to characterize the performance of a device, system, or method, relative to its alternatives. In analytical calibration, figures of merit are employed to compare the relative performances of different analytical methodologies and also to establish detection capabilities, a feature which is specific for analytical chemistry. Focus is first directed to the sensitivity, which has been shown to be a key parameter in the estimation of the remaining figures of merit. A single and general sensitivity equation is as follows:

$$\text{SEN}_n = \left\{\mathbf{g}_n^T\left[\mathbf{Z}_{exp}^T\left(\mathbf{I} - \mathbf{Z}_{unx}\mathbf{Z}_{unx}^+\right)\mathbf{Z}_{exp}\right]^{-1}\mathbf{g}_n\right\}^{-1/2} \quad (17)$$

One important factor in Eq. (17) is the so-called analyte selector ($\mathbf{g}_n$), a vector of numbers. In PLS/RBL, it is a vector of numbers which adequately combines the calibration information (latent loadings) to make it specific for the analyte of interest (the $\mathbf{v}$ vector of latent regression coefficients). The second important information in Eq. (17) is the matrix $\mathbf{Z}_{exp}$, which is a function of the profiles (calibration loadings) retrieved by the algorithm for the expected components. Finally, Eq. (17) includes a matrix containing information on the unexpected components, $\mathbf{Z}_{unx}$, defined as a function of the profiles recovered for the potential interferents (in RTL they may be abstract profiles).

Selectivity is the extent to which a method can be used to determine particular analytes in mixtures or matrices without interferences from other components of similar behavior. In multi-way calibration, it is possible to assign a numerical parameter to the selectivity, defining the latter as the portion of the analyte signal employed for quantitation, i.e., as the ratio between the sensitivity and the slope of the pseudo-univariate calibration graph:

$$\text{SEL} = \text{SEN}/s_n \quad (18)$$

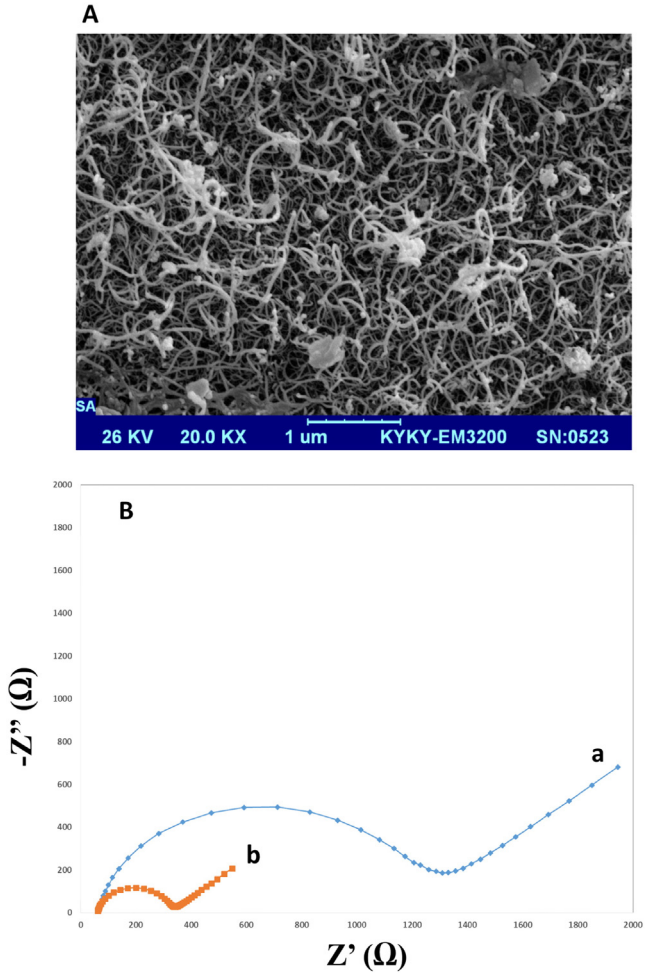

Fig. 1. (A) SEM image of MWCNTs/GCE, and (B) electrochemical impedance spectra of bare GCE (curve a) and MWCNTs/GCE (curve b).

One potential problem with the interpretation of the sensitivity is that it depends on the specific type of signal employed for developing a calibration method. The value of SEN has units of (signal × concentration^{-1}), and therefore, sensitivities derived from spectral and electrochemical measurements cannot be compared on an equal basis. For these reasons, the analytical sensitivity, sometimes called γ, has been proposed and defined as the ratio between sensitivity and instrumental noise:

$$\gamma = \mathrm{SEN}/\sigma_x \quad (19)$$

where σ_x is an estimation of the degree of noise level in the measured instrumental signals.

The modern definition of limit of detection (LOD), based on IUPAC's recommendations, is the minimum concentration that can be reliably detected by the method. The LOD can be estimated as 3.3 times the standard deviation for a sample of low or zero analyte concentration and can be given by

$$\mathrm{LOD} = 3.3\sigma_0 \quad (20)$$

3. Results and discussion

3.1. Characterization of MWCNTs/GCE

The SEM image of MWCNTs/GCE (Fig. 1A) shows that MWCNTs twining around each other and attached to the GCE. It is clear that MWCNTs almost homogeneously distributed on the electrode surface by forming a thin layer. Electrochemical impedance spectroscopy (EIS) has been considered as an effective technique for the impedance investigation of bare GCE and MWCNTs/GCE. The EIS experiments were carried out in a supporting electrolyte solution of 1.0 M KCl containing equimolar $[Fe(CN)_6]^{4-/3-}$ in a frequency range from 0.1 to 100.0 kHz. The semicircle is interrelated to the charge-transfer resistance process (R_{ct}), and the oblique line that defines a region of semi-infinite diffusion of analytes in the electrode corresponds to the Warburg impedance. As can be observed in Fig. 1B, it is concluded that the R_{ct} of the MWCNTs/GCE (curve b) is smaller than that of the bare GCE (curve a). Therefore, by modification of GCE with MWCNTs, the bulk resistance decreases. This result suggests that the electron transfer is easier at the surface of MWCNTs/GCE.

3.2. pH dependence study

To select the best pH for the simultaneous determination of LD, CD, MD, AC, TRA, LC, TOP, OF, LOF, and NOF, the effect of pH on the peak current of their DPVs was investigated. Fig. 2A–J shows the influence of the pH of the PBS (0.1 mol L^{-1}), in the range of 2.0–10.0, on the signal intensities of each analyte. As can be observed, all peak currents of the studied analytes have a maximum value at pH 3.0. Taking into account that for analytical purposes, both maximal and stable currents are necessary, a pH value of 3.0 was selected for further experiments. The oxidation peak potential of all studied analytes shifted to less positive values as the pH of the buffer solution was increased (Fig. 2A–J).

3.3. Calibrations

3.3.1. Univariate calibrations

Prior to multivariate calibration experiments, univariate calibration experiments were performed (Fig. 3A–J) in order to check the linear analytical range for the isolated analytes. Solutions for calibration curves were prepared by convenient dilution of the standard solutions with PBS (0.1 mol L^{-1}, pH 3.0). Calibration curves were constructed with several points as peak current versus analyte concentration and fitted by standard least-squares regression. The linear ranges of calibration curves were the limiting assayed concentrations in subsequent analyses. All analytes showed linear dependences between peak current and concentration at different concentration intervals. As can be seen, a strong signal overlapping was observed for the simultaneous analysis of LD, CD, MD, AC, TRA, LC, TOP, OF, LOF, and NOF (see Fig. 3), and quantification of any of them will be biased if univariate calibration is used as analytical method. Thus, in complex cases such as the present one, it is necessary to employ advanced multivariate calibration techniques such as multi-way multivariate calibration. Third-order multivariate calibration is known to provide increased sensitivity and selectivity but, up to now, this technique has not been used for electrochemical data, and no electrochemical data have been reported for application to four-way multivariate calibration.

3.3.2. Multivariate calibrations

A calibration set of 23 samples containing LD, CD, MD, AC, TRA, LC, TOP, OF, LOF, and NOF was prepared in PBS (0.1 mol L^{-1}, pH 3.0) according to a central composite design (Table 1) and considering the

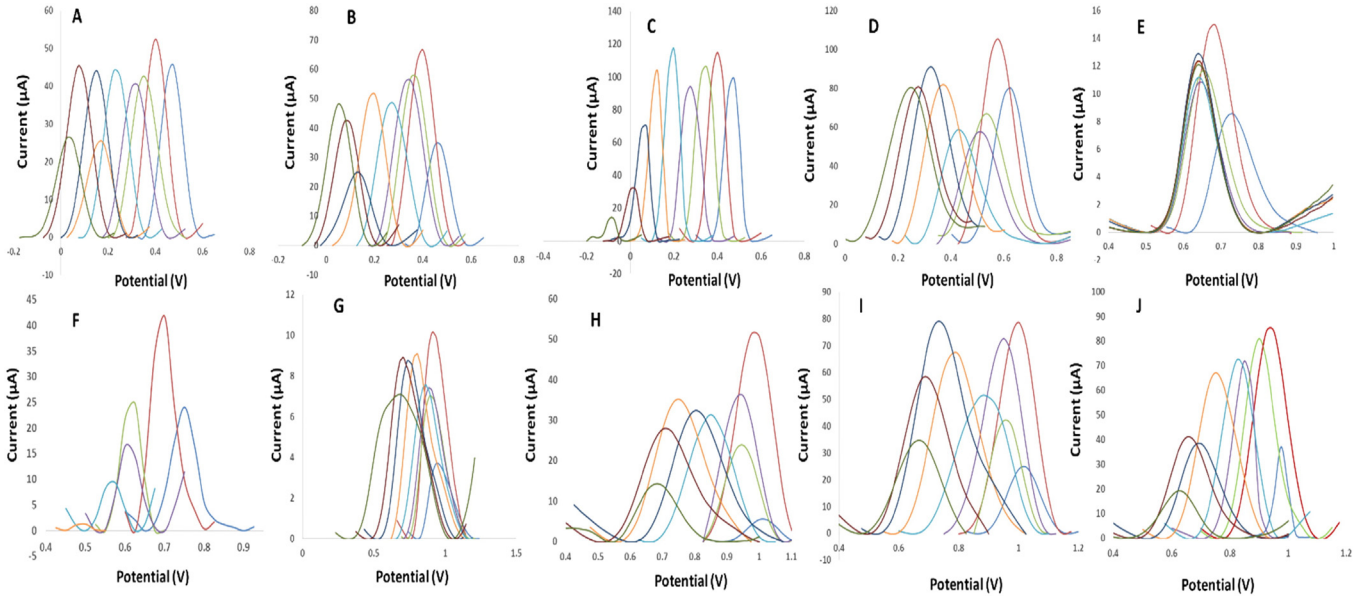

Fig. 2. Differential pulse voltammograms of (A) LD (4.0×10^{-3} mol L^{-1}), (B) CD (2.0×10^{-4} mol L^{-1}), (C) MD (5.0×10^{-3} mol L^{-1}), (D) AC (5.5×10^{-3} mol L^{-1}), (E) TRA (0.8×10^{-3} mol L^{-1}), (F) LC (1.0×10^{-3} mol L^{-1}), (G) TOP (1.3×10^{-3} mol L^{-1}), (H) OF (8.0×10^{-3} mol L^{-1}), (I) LOF (8.0×10^{-3} mol L^{-1}), and (J) NOF (5.0×10^{-3} mol L^{-1}) in 0.1 mol L^{-1} PBS at different pHs.

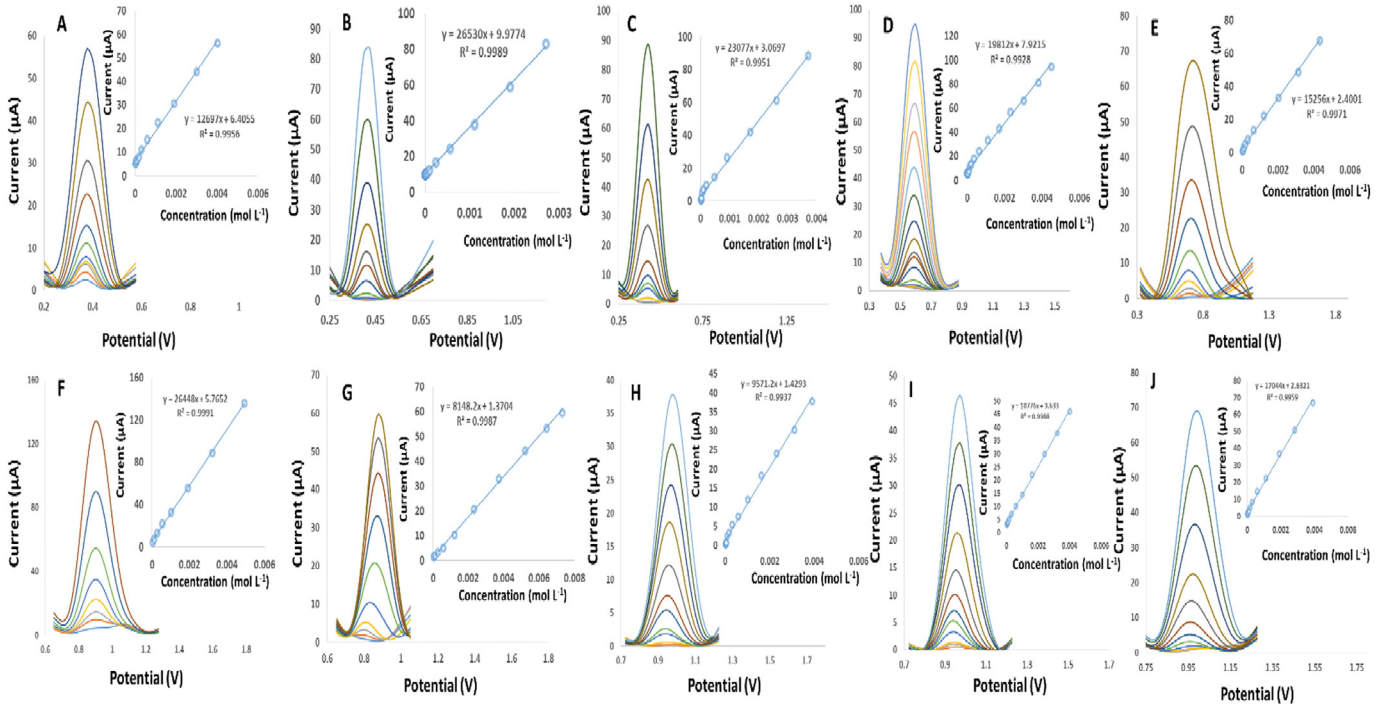

Fig. 3. Representative differential pulse voltammograms of (A) LD, (B) CD, (C) MD, (D) AC, (E) TRA, (F) LC, (G) TOP, (H) OF, (I) LOF, and (J) NOF in PBS (0.1 mol L^{-1}, pH 3.0) at different concentrations. Insets: dependence of I_p with concentration.

Table 1
Composition of the samples used in the calibration and test sets.

Calibration set

	Analytes (10^{-6} mol L^{-1})									
Sample	**LD**	**CD**	**MD**	**AC**	**TRA**	**LC**	**TOP**	**OF**	**LOF**	**NOF**
1	4000	2700	0.5	4480	4300	20	7300	1	5	5
2	4000	0.05	3700	4480	9.99	4900	20	1	5	3900
3	4000	0.05	0.5	0.5	4300	4900	7300	1	4000	3900
4	5	0.05	3700	4480	4300	20	7300	3900	5	3900
5	5	2700	3700	0.5	4300	20	20	1	4000	3900
6	5	0.05	0.5	0.5	9.99	20	20	1	5	5
7	4000	0.05	3700	0.5	9.99	20	7300	3900	4000	5
8	4000	2700	0.5	4480	9.99	20	20	3900	4000	3900
9	5	2700	0.5	0.5	9.99	4900	7300	3900	5	3900
10	4000	2700	3700	0.5	4300	4900	20	3900	5	5
11	5	0.05	0.5	4480	4300	4900	20	3900	4000	5
12	5	2700	3700	4480	9.99	4900	7300	1	4000	5
13	0	0	0	0	0	0	0	0	0	0
14	5	0	0	0	0	0	0	0	0	0
15	0	0.05	0	0	0	0	0	0	0	0
16	0	0	0.5	0	0	0	0	0	0	0
17	0	0	0	0.5	0	0	0	0	0	0
18	0	0	0	0	9.99	0	0	0	0	0
19	0	0	0	0	0	20	0	0	0	0
20	0	0	0	0	0	0	20	0	0	0
21	0	0	0	0	0	0	0	1	0	0
22	0	0	0	0	0	0	0	0	5	0
23	0	0	0	0	0	0	0	0	0	5

Test set

	Analytes (10^{-6} mol L^{-1})										Interferences (10^{-6} mol L^{-1})		
Sample	**LD**	**CD**	**MD**	**AC**	**TRA**	**LC**	**TOP**	**OF**	**LOF**	**NOF**	**BA**	**DP**	**COF**
1	6	12	2	8	2	5	3	1	4	2	45	148	211
2	12	21	76	47	33	88	28	36	15	21	115	122	156
3	48	78	54	69	24	41	11	23	43	33	33	88	56
4	33	32	5	12	55	76	21	21	31	65	168	35	133
5	18	45	85	48	12	115	54	12	12	54	54	41	95
6	41	18	32	87	5	21	33	8	8	32	41	78	41
7	38	39	45	10	8	36	5	28	19	29	123	12	23
8	8	78	51	36	38	65	41	33	38	59	88	134	68
9	44	66	66	55	41	98	50	18	21	43	95	90	88
10	54	54	17	60	18	130	55	9	10	50	11	45	12

linear ranges which previously established from univariate calibrations for each analyte. A test set of 10 synthetic mixtures containing random concentrations of LD, CD, MD, AC, TRA, LC, TOP, OF, LOF, and NOF was prepared in PBS (0.1 mol L^{-1}, pH 3.0) to which BA, DP, and COF were added with random concentrations as uncalibrated interferences (Table 1). In both calibration and test sets, for each sample, six pulse durations of 0.0078–0.0468 s with a 0.0078 s interval were assigned and for each pulse duration, six DPVs were recorded at different pulse heights of 0.0031–0.0191 V with a 0.0031 V interval.

3.4. Data pretreatments

In our previous works [44–47], we pointed out that voltammetric performance can be enhanced by data pretreatments. Besides the problem arising from the presence of severely overlapping analyte profiles, in the present study, two additional complications may occur: (1) the baselines and (2) sample-to-sample potential shifts in the analyte profiles, which are common in voltammetric studies. For tackling the first problem, it was necessary to eliminate the baselines by the method proposed by Eilers et al. [48,49]. Concerning the second of the above commented problems, the potentials shifts were corrected by COW [40]. For more understanding about the details of the baseline- and shift-correction techniques, the reader is referred to Refs. [40,48,49].

Regarding the problems mentioned above, the matrices of the raw data were placed next to each other (Fig. 4A) to obtain an expanded matrix and then this expanded matrix was submitted to baseline correction (Fig. 4B) and potential shift correction (Fig. 4C). The pre-treated data (baseline- and potential shift-corrected data) was then mathematically assembled using MATLAB commands to restore their original format (four-way data array) and used for next computations.

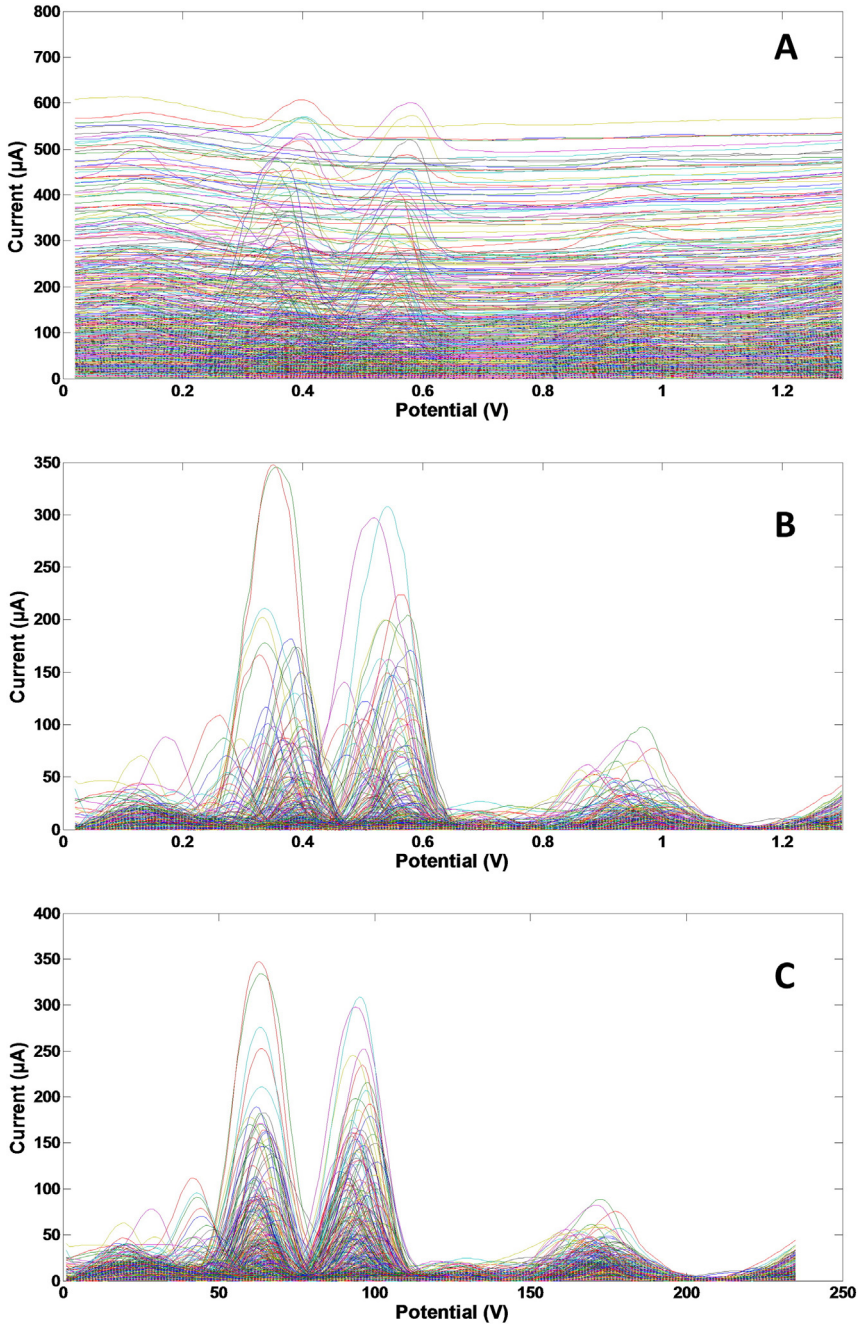

Fig. 4. Differential pulse voltammetric data corresponding to the calibration set. (A) Raw data, and after preprocessing: (B) baseline correction and (C) alignment with COW.

Table 2
Predicted concentrations for the test set by U-PLS/RTL and N-PLS/RTL.

U-PLS/RTL	Analytes (10^{-6} mol L^{-1})									
Sample	**LD**	**CD**	**MD**	**AC**	**TRA**	**LC**	**TOP**	**OF**	**LOF**	**NOF**
1	6.1	11.8	1.95	8.05	2.09	5.04	2.92	1.01	4.05	2.02
2	12.1	21.2	75.3	46.4	36.5	89.1	28.3	35.6	14.88	21.3
3	47.3	77.6	55.1	68.4	23.5	41.2	11.2	23.3	43.3	33.6
4	32.6	31.54	5.03	11.9	54.4	76.6	20.9	21.2	31.1	65.4
5	18.1	45.4	83.89	47.3	11.95	114.5	53.4	12.1	12.1	54.1
6	41.34	18.1	31.45	88.1	4.83	20.9	33.2	8.2	7.81	32.3
7	37.5	39.2	44.3	10.1	7.21	35.8	5.02	27.8	18.4	29.2
8	8.06	78.3	50.4	35.6	34.3	64.5	41.2	33.1	38.2	59.4
9	44.2	65.4	66.5	54.3	49.9	99.1	49.8	18.2	21.3	43.5
10	53.3	53.8	17.1	59.8	17.89	129.8	54.3	8.9	9.91	50.2
RMSEP[a]	0.39	0.33	0.65	0.55	0.45	0.58	0.33	0.20	0.25	0.34
REP[b]	1.31	0.76	1.52	1.29	1.93	0.86	1.11	1.10	1.27	0.89
N-PLS/RTL	Analytes (10^{-6} mol L^{-1})									
Sample	**LD**	**CD**	**MD**	**AC**	**TRA**	**LC**	**TOP**	**OF**	**LOF**	**NOF**
1	6.98	12.95	2.2	8.88	2.3	5.45	3.28	1.12	4.78	2.21
2	10.99	23.1	79.1	49.3	36.3	91.3	29.99	38.94	16.73	23.43
3	45.8	80.6	55.9	70.9	25.6	44.5	11.92	21.1	41.2	31.04
4	31.2	31.3	3.99	13.3	12.9	73.3	20.1	23.88	33.6	62.34
5	19.6	47.8	83.1	50.6	6.02	121.4	52.3	13.2	12.95	52.1
6	40.1	19.2	34.2	90.2	8.88	23.33	30.88	9.08	6.98	30.3
7	36.1	37.1	47.3	11.2	40.3	33.2	5.95	29.66	17.4	31.4
8	6.99	76.3	53	33.4	38.7	68.4	39.3	31.2	36.1	60.3
9	42.1	69.1	63.9	53.6	44.1	100.2	48.2	20.1	23.3	45.89
10	56.2	57.2	18.3	63.7	19.8	133.6	57.6	10.1	11.1	47.76
RMSEP[a]	1.62	2.19	1.95	2.28	17.00	3.37	1.63	1.86	1.67	2.11
REP[b]	5.39	4.95	4.50	5.28	72.07	5.00	5.44	9.86	8.35	5.41

[a] RMSEP, root mean square error prediction in 10^{-6} mol L^{-1}.
[b] REP, relative error prediction in %.

3.5. U-PLS/RTL and N-PLS/RTL applied to the third-order data

The first step is the assessment of the correct number of sample constituents or the latent variables. For U-PLS/RTL and N-PLS/RTL, a leave-one-sample-out cross-validation procedure, according to the criterion of Haaland and Thomas [42], was performed. In these two algorithms, the optimal number of factors was estimated by calculating the ratios $F(A) = \text{PRESS}(A < A^*) / \text{PRESS}(A)$ [where $\text{PRESS} = \Sigma(y_{i,act} - y_{i,pred})^2$, A is a trial number of factors ,and A^* corresponds to the minimum PRESS] and selecting the number of factors leading to a probability of

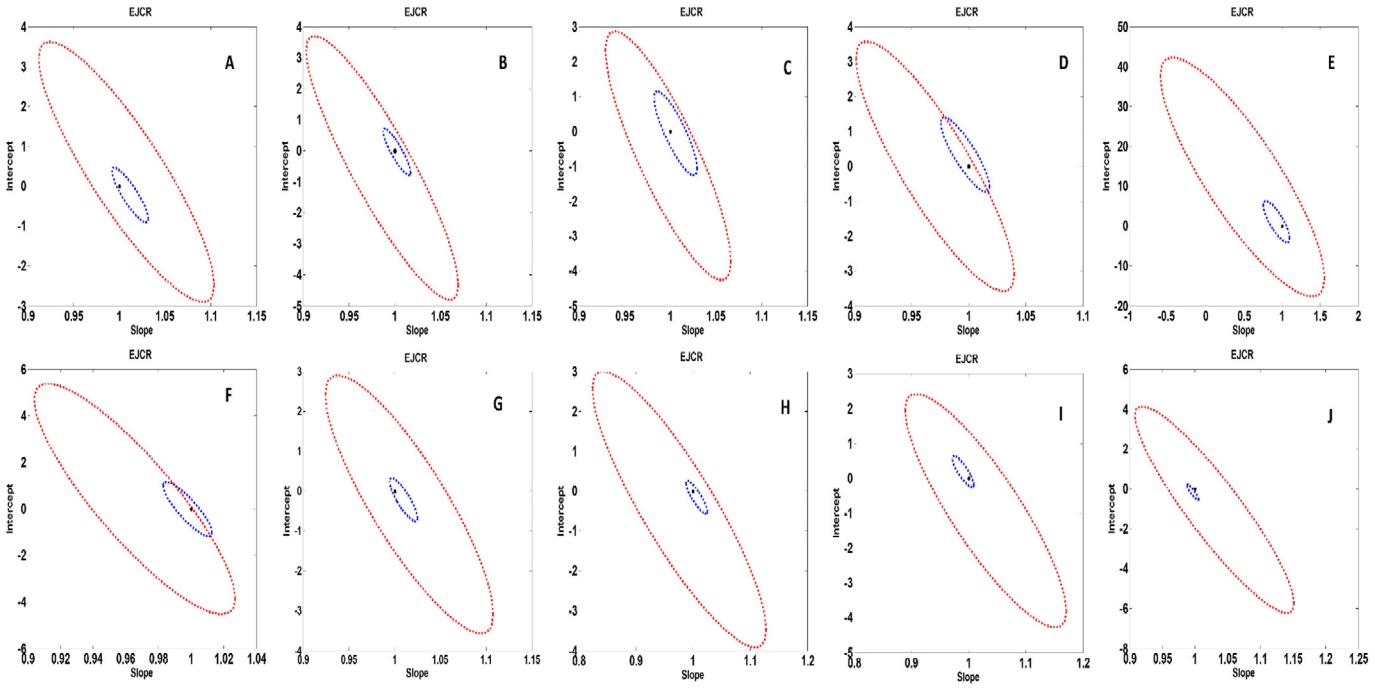

Fig. 5. Elliptical joint regions (at 95% confidence level) for the slopes and intercepts of the regressions for (A) LD, (B) CD, (C) MD, (D) AC, (E) TRA, (F) LC, (G) TOP, (H) OF, (I) LOF, and (J) NOF in test set. Black point marks the theoretical (0,1) point. In all cases, red and blue ellipses are related to N-PLS/RTL and U-PLS/RTL, respectively.

Table 3
Analytical figures of merit for U-PLS/RTL method in the test samples.

	Analytes									
AFOM	**LD**	**CD**	**MD**	**AC**	**TRA**	**LC**	**TOP**	**OF**	**LOF**	**NOF**
SEN[a]/μA μM^{-1}	0.12	0.08	0.16	0.21	0.18	0.31	0.16	0.22	0.15	0.25
SEL[b]	0.34	0.26	0.23	0.38	0.41	0.25	0.33	0.29	0.36	0.23
(γ^{-1})[c]/μM	0.04	0.01	0.06	0.08	0.05	0.09	0.05	0.1	0.09	0.11
LOD[d]/μM	4.5	0.03	0.4	0.1	2.3	12	10	0.32	2.5	2.1

[a] SEN, sensitivity.
[b] SEL, selectivity.
[c] γ^{-1}, inverse of analytical sensitivity (represents the minimum concentration difference which can be measured).
[d] LOD, limit of detection.

less than 75% that F > 1. For the two calibration models, the estimated number of components was 10, which can be justified taking into account the presence of the ten analytes.

The predicted concentrations corresponding to the application of U-PLS/RTL and N-PLS/RTL in the analysis of test samples and the statistical parameters (RMSEPs and REPs) are collected in Table 2. It is noticeable that the results obtained with N-PLS/RTL are not good. However, the results obtained with U-PLS/RTL are very satisfactory. This may be an indication that U-PLS/RTL may be better prepared to cope with the problems of severe overlapping.

3.6. Comparison of predictive ability of U-PLS/RTL and N-PLS/RTL

In order to compare the predictive ability of the third-order algorithms, the predicted concentrations of the test set (Table 2) were regressed on the nominal concentrations. In this case, an ordinary least squares (OLS) analysis of predicted concentrations versus nominal concentrations was applied [50]. The calculated intercept and slope were compared with their theoretically expected values (intercept = 0, slope = 1), based on the elliptical joint confidence region (EJCR) test. If the ellipses contain the values 0 and 1 for intercept and slope (ideal point), respectively, showing that the predicted and nominal values do not present significant difference at the level of 95% confidence and the elliptic size denotes precision of the analytical method, smaller size corresponds to higher precision [51]. Fig. 5 A–J shows the corresponding ellipses of the EJCR analyses. As can be concluded from Fig. 5 A–J, the best predictions (smaller ellipses) were obtained by U-PLS/RTL, which show the accurate determination of analytes by the developed methodology. If the EJCRs for NOF determination are analyzed (Fig. 5J), it is notable that the ideal point falls on the blue ellipse, denoting slightly poorer prediction accuracy for NOF rather than other analytes.

The results of EJCR test demonstrated the more superiority of U-PLS/RTL to resolve the complex systems, therefore, further analysis of the results of N-PLS/RTL will not be performed and we will focus on U-PLS/RTL. Analytical figures of merit (AFOM) for the proposed U-PLS/RTL method including sensitivity (SEN), inverse of analytical sensitivity (γ^{-1}), selectivity (SEL), and limit of detection (LOD) are summarized in Table 3. From Table 3, all parameters are seen to be good, indicating that the U-PLS/RTL model offers a very sensitive and selective method for simultaneous determination of LD, CD, MD, AC, TRA, LC, TOP, OF, LOF, and NOF even in the presence of uncalibrated interferences.

3.7. Analysis of human serum samples

In view of the above results, U-PLS/RTL was selected as the algorithm to be applied to real samples. To evaluate the feasibility of the proposed method, simultaneous quantification of LD, CD, MD, AC, TRA, LC, TOP, OF, LOF, and NOF in the presence of BA, DP, and COF was performed in partially diluted human serum samples. Serum samples were partially diluted with PBS (0.1 mol L^{-1}, pH 3.0) and spiked with different amounts of the analytes and interferences. Then, aliquots of the diluted samples were introduced into the electrochemical cell. For each sample, six pulse durations of 0.0078–0.0468 s with a 0.0078 s interval were assigned, and for each pulse duration, six DPVs were recorded in six different pulse heights of 0.0031–0.0191 V with a 0.0031 V interval. The recovery rates of the spiked samples were achieved between 96.73% and 103.65%, showing the success of the proposed methodology for simultaneous determination of LD, CD, MD, AC, TRA, LC, TOP, OF, LOF, and NOF in blood serum which has a very complex matrix (Table 4).

4. Conclusion

This study describes a very attractive methodology for the simultaneous determination of LD, CD, MD, AC, TRA, LC, TOP, OF, LOF, and NOF in the presence of BA, DP, and COF as uncalibrated interferences at the surface of MWCNTs/GCE by recording third-order DPV data and applying two third-order algorithms such as U-PLS/RTL and N-

Table 4
Results of simultaneous determination of LD, CD, MD, AC, TRA, LC, TOP, OF, LOF, and NOF in human serum sample by U-PLS/RTL.

Sample	Added (10^{-6} mol L^{-1})												
	LD	**CD**	**MD**	**AC**	**TRA**	**LC**	**TOP**	**OF**	**LOF**	**NOF**	**BA**	**DP**	**COF**
1	230	110	170	550	60	55	111	66	231	100	120	40	150
2	75	240	120	311	120	135	55	70	50	85	85	66	41
3	440	66	95	200	89	180	88	55	90	78	34	51	34
Sample	Found (10^{-6} mol L^{-1})												
	LD	**CD**	**MD**	**AC**	**TRA**	**LC**	**TOP**	**OF**	**LOF**	**NOF**			
1	228	112.3	172.1	547.1	58.8	55.3	109.2	67.3	233	98.4			
2	73.3	238.7	123.9	314.7	123.5	133.2	56.4	71.7	48.4	87.2			
3	441.3	68.5	97.4	198.7	87.6	178.3	86.4	53.2	88.4	76.5			
Sample	Recovery (%)												
	LD	**CD**	**MD**	**AC**	**TRA**	**LC**	**TOP**	**OF**	**LOF**	**NOF**			
1	99.14	102.04	101.22	99.47	98	100.54	98.38	101.93	100.86	98.4			
2	97.73	99.46	103.15	101.17	102.83	98.67	102.48	102.37	96.8	102.52			
3	100.29	103.65	102.46	99.35	98.43	99.06	98.18	96.73	98.22	98.08			

PLS/RTL. The main goals of this work were (i) to create third-order voltammetric data and (ii) to perform the analysis in the presence of an unexpected interference. To achieve the first goal, third-order DPV data were recorded using simple changes in pulse height and pulse duration of DPV signals, and to achieve the second one, a comparison was made between U-PLS/RTL and N-PLS/RTL as two well-known third-order algorithms to choose the best one for the analysis of real samples. The recorded four-way data array was non-bilinear, trilinear, and non-quadrilinear, therefore, the non-linearities were tackled by potential shift correction using COW as a well-known chemometric tool. Among the third-order algorithms analyzed, U-PLS/RTL showed the best results for determination of the analytes even in the presence of unexpected interferences. The better performance of U-PLS/RTL is due to the fact that the U-PLS/RTL model is a much more complex and flexible model than N-PLS/RTL. The use of four-way data array, exploiting the information contained in full voltammetric matrices and third-order algorithms, allowed the successful simultaneous determination of ten analytes in both synthetic and real samples even in the presence of unexpected interferences. The proposed methodology in this study exploited the second-order advantage and also demonstrated that combination of voltammetric measurements with four-way multivariate calibration method turned possible the simultaneous determination of LD, CD, MD, AC, TRA, LC, TOP, OF, LOF, and NOF in the presence of BA, DP, and COF as uncalibrated interferences in complex matrices such as human serum, despite the serious interference from the background components. The potential advantages of the proposed method in this study (U-PLS/RTL), such as sensitivity, rapidity, and low-cost, can be even more highlighted by considering the possibility of it for biosensing and clinical applications.

Acknowledgements

The authors wish to express their sincere appreciation to Razi University Research Council for financial support of this project. ARJ gives thanks to GOD for the opportunity of life and spending it for education and is also so happy to do this work as the last project of his Ph.D. course.

References

[1] K.S. Booksh, B.R. Kowalski, Theory of analytical chemistry, Anal. Chem. 66 (1994) 782–791.
[2] H. Wold, E. Lyttkens, Nonlinear iterative partial least squares (nipals) estimation procedures, Bull. Intern. Statist. Inst. Proc., London1969.
[3] S. Wold, A. Ruhe, H. Wold, W.J. Dunn, The collinearity problem in linear regression: the partial least squares approach to generalized inverses, SIAM J. Sci. Stat. Comput. 5 (1984) 735–743.
[4] P.J. Gemperline, A priori estimates of the elution profiles of the pure components in overlapped liquid chromatography peaks using target factor analysis, J. Chem. Inf. Comput. Sci. 24 (1984) 206–212.
[5] Y.Z. Liang, O.M. Kvalheim, H.R. Heller, D.L. Massart, P. Kiechle, F. Erni, Heuristic evolving latent projections: resolving two-way multicomponent data. 2. Detection and resolution of minor constituents, Anal. Chem. 64 (1992) 946–953.
[6] B. Walczak, D.L. Massart, Robust principal components regression as a detection tool for outliers, Chemom. Intell. Lab. Syst. 27 (1995) 41–54.
[7] P.J. Gemperline (Ed.), Practical guide to chemometrics, CRC Press, Boca Raton, 2006.
[8] S. Wold, K. Esbensen, P. Geladi, Principal component analysis, Chemom. Intell. Lab. Syst. 2 (1987) 37–52.
[9] L.X. Zhang, W. Fan, D.S. Cao, M.M. Zeng, H.B. Xiao, Y.Z. Liang, Neutral losses: a type of important variables in prediction of branching degree for acyclic alkenes from mass spectra, Anal. Chim. Acta 720 (2012) 16–21.
[10] A. Durand, O. Devos, C. Ruckebusch, J.P. Huvenne, Genetic algorithm optimisation combined with partial least squares regression and mutual information variable selection procedures in near-infrared quantitative analysis of cotton–viscose textiles, Anal. Chim. Acta 595 (2007) 72–79.
[11] B. Üstün, W.J. Melssen, M. Oudenhuijzen, L.M.C. Buydens, Determination of optimal support vector regression parameters by genetic algorithms and simplex optimization, Anal. Chim. Acta 544 (2005) 292–305.
[12] K. Héberger, A.P. Borosy, Comparison of chemometric methods for prediction of rate constants and activation energies of radical addition reactions, J. Chemom. 13 (1999) 473–489.
[13] X. Huang, Q.S. Xu, Y.Z. Liang, PLS regression based on sure independence screening for multivariate calibration, Anal. Methods 4 (2012) 2815–2821.
[14] E. Sánchez, B.R. Kowalski, Generalized rank annihilation factor analysis, Anal. Chem. 58 (1986) 496–499.
[15] E. Sánchez, B.R. Kowalski, Tensorial resolution: a direct trilinear decomposition, J. Chemom. 4 (1990) 29–45.
[16] L. Xia, H.L. Wu, S.F. Li, S.H. Zhu, L.Q. Hu, R.Q. Yu, Alternating penalty quadrilinear decomposition algorithm for an analysis of four-way data arrays, J. Chemom. 21 (2007) 133–144.
[17] P.C. Damiani, I. Duran-Meras, A. Garcıa-Reiriz, A. Jimenez-Giron, A.M. Pena, A.C. Olivieri, Multiway partial least-squares coupled to residual trilinearization: a genuine multidimensional tool for the study of third-order data. simultaneous analysis of procaine and its metabolite p-aminobenzoic acid in equine serum, Anal. Chem. 79 (2007) 6949–6958.
[18] R.P.H. Nikolajsen, K.S. Booksh, A.M. Hansen, R. Bro, Quantifying catecholamines using multi-way kinetic modelling, Anal. Chim. Acta 475 (2003) 137–150.
[19] J.A. Arancibia, A.C. Olivieri, D.B. Gil, A.E. Mansilla, I. Duran-Meras, A. Muñoz de la Peña, Trilinear least-squares and unfolded-PLS coupled to residual trilinearization: new chemometric tools for the analysis of four-way instrumental data, Chemom. Intell. Lab. Syst. 80 (2006) 77–86.
[20] H.C. Goicoechea, S.j. Yu, A.C. Olivieri, A.D. Campiglia, Four-way data coupled to parallel factor model applied to environmental analysis: determination of 2,3,7,8-tetrachloro-dibenzo-para-dioxin in highly contaminated waters by solid-liquid extraction laser-excited time-resolved Shpol'skii spectroscopy, Anal. Chem. 77 (2005) 2608–2616.
[21] A.M. de la Pena, I.D. Meras, A.J. Giron, H.C. Goicoechea, Evaluation of unfolded-partial least-squares coupled to residual trilinearization for four-way calibration of folic acid and methotrexate in human serum samples, Talanta 72 (2007) 1261–1268.
[22] S.E.G. Porter, D.R. Stoll, S.C. Rutan, P.W. Carr, J.D. Cohen, Analysis of four-way two-dimensional liquid chromatography-diode array data: application to metabolomics, Anal. Chem. 78 (2006) 5559–5569.
[23] A.C. Olivieri, J.A. Arancibia, A.M. Pena, I. Duran-Meras, A.E. Mansilla, Second-order advantage achieved with four-way fluorescence excitation — emission — kinetic data processed by parallel factor analysis and trilinear least-squares. Determination of methotrexate and leucovorin in human urine, Anal. Chem. 76 (2004) 5657–5666.
[24] X.Q. Chen, Y.Y. Jin, G. Tang, New Pharmacology, People's Medical Publishing House, Beijing, 2003.
[25] N.L. Benowitz, Basic and Clinical Pharmacology, The McGraw-Hill Companies, New York, 2004.
[26] The United States Pharmacopoeia, Rand McNally, Taunton, MA, 1995.
[27] D.R.C. Robertson, A.G. Renwick, B. Macklin, S. Jones, D.G. Waller, C.F. George, J.S. Fleming, The influence of levodopa on gastric emptying in healthy elderly volunteers, Eur. J. Clin. Pharmacol. 42 (1992) 409–412.
[28] B.J. Sanghavi, A.K. Srivastava, Simultaneous voltammetric determination of acetaminophen and tramadol using Dowex50wx2 and gold nanoparticles modified glassy carbon paste electrode, Anal. Chim. Acta 706 (2011) 246–254.
[29] S. Liawruangrath, B. Liawruangrath, P. Pibool, Simultaneous determination of tolperisone and lidocaine by high performance liquid chromatography, J. Pharm. Biomed. Anal. 26 (2001) 865–872.
[30] J. Pórszász, K. Nador, K.G. Pórszász, T. Barankay, Pharmakologie einer neuen interneuron-lahmenden substanz 1-Piperidino-2-Methyl-3-(P-Tolyl)-Propan-3-on, Arzneimittel-Forschung, Drug Res. 11 (1961) 257–260.
[31] P. Bajaj, L. Arendt-Nielsen, P. Madeleine, P. Svensson, Prophylactic tolperisone for post-exercise muscle soreness causes reduced isometric force-adouble-blind randomized crossover control study, Eur. J. Pain 7 (2003) 407–418.
[32] P. Svensson, K. Wang, L. Arendt-Nielsen, Effect of muscle relaxants on experimental jaw-muscle pain and jaw-stretch reflexes: a double-blind and placebo-controlled trial, Eur. J. Pain 7 (2003) 449–456.
[33] C.I. Choi, J.I. Park, H.I. Lee, Y.J. Lee, C.G. Jang, J.W. Bae, S.Y. Lee, Determination of tolperisone in human plasma by liquid chromatography/tandem mass spectrometry for clinical application, J. Chromatogr. B 911 (2012) 59–63.
[34] T. Uematsu, M. Nakashima, in: S. Mitsuhashi (Ed.), Progress in Drug Research, Birkhaeuser Verlag, Base, 1992.
[35] F. Valentini, A. Amine, S. Orlanducci, M.L. Terranova, G. Palleschi, Carbon nanotube purification: preparation and characterization of carbon nanotube paste electrodes, Anal. Chem. 75 (2003) 5413–5421.
[36] J.H. Suh, Y.Y. Lee, H.J. Lee, M. Kang, Y. Hur, S.N. Lee, D.H. Yang, S.B. Han, Dispersive liquidp-liquid microextraction based on solidification of floating organic droplets followed by high performance liquid chromatography for the determination of duloxetine in human plasma, J. Pharm. Biomed. Anal. 75 (2013) 214–219.
[37] L.R. Faulkner, A.J. Bard, Electrochemical methods: fundamental and application, Wiley, New York, 2001.
[38] M. Kooshki, H. Abdollahi, S. Bozorgzadeh, B. Haghighi, Second-order data obtained from differential pulse voltammetry: Determination of tryptophan at a gold nanoparticles decorated multiwalled carbon nanotube modified glassy carbon electrode, Electrochim. Acta 56 (2011) 8618–8624.
[39] H. Abdollahi, M. Kooshki, Second-order data obtained from differential pulse voltammetry: determination of lead in river water using multivariate curve resolution-alternating least-squares (MCR-ALS), Electroanalysis 22 (2010) 2245–2253.
[40] G. Tomasi, F. Savorani, S.B. Engelsen, icoshift: an effective tool for the alignment of chromatographic data, J. Chromatogr. A 1218 (2011) 7832–7840.
[41] S. Wold, P. Geladi, K. Esbensen, J. Øhman, Multi-way principal components- and PLS-analysis, J. Chemom. 1 (1987) 41–56.
[42] D.M. Haaland, E.V. Thomas, Partial least-squares methods for spectral analyses. 1. Relation to other quantitative calibration methods and the extraction of qualitative information, Anal. Chem. 60 (1988) 1193–1202.
[43] R. Bro, Multi-way Analysis in the Food Industry, University of Amsterdam, Netherlands, 1998 Doctoral Thesis.

[44] M.B. Gholivand, A.R. Jalalvand, H.C. Goicoechea, Th. Skov, Chemometrics-assisted simultaneous voltammetric determination of ascorbic acid, uric acid, dopamine and nitrite: application of non-bilinear voltammetric data for exploiting first-order advantage, Talanta 119 (2014) 553–563.
[45] M.B. Gholivand, A.R. Jalalvand, H.C. Goicoechea, R. Gargallo, Th. Skov, G. Paimard, Combination of electrochemistry with chemometrics to introduce an efficient analytical method for simultaneous quantification of five opium alkaloids in complex matrices, Talanta 131 (2015) 26–37.
[46] A.R. Jalalvand, M.B. Gholivand, H.C. Goicoechea, Th. Skov, Generation of non-multilinear three-way voltammetric arrays by an electrochemically oxidized glassy carbon electrode as an efficient electronic device to achieving second-order advantage: Challenges, and tailored applications, Talanta 134 (2015) 607–618.
[47] A.R. Jalalvand, M.B. Gholivand, H.C. Goicoechea, Å. Rinnan, Th. Skov, Advanced and tailored applications of an efficient electrochemical approach assisted by AsLSSR-COW-rPLS and finding ways to cope with challenges arising from the nature of voltammetric data, Chemom. Intell. Lab. Syst. 146 (2015) 437–446.
[48] P.H.C. Eilers, Parametric time warping, Anal. Chem. 76 (2004) 404–411.
[49] P.H.C. Eilers, I.D. Currie, M. Durban, Fast and compact smoothing on large multidimensional grids, Comput. Stat. Data An. 50 (2006) 61–76.
[50] A.G. Gonzalez, M.A. Herrador, A.G. Asuero, Intra-laboratory testing of method accuracy from recovery assays, Talanta 48 (1999) 729–736.
[51] J.A. Arancibia, G.M. Escandar, Two different strategies for the fluorimetric determination of piroxicam in serum, Talanta 60 (2003) 1113–1121.